Science Translational Medicine
AAAS

Blockade of Nonhormonal Fibroblast Growth Factors by FP-1039 Inhibits Growth of Multiple Types of Cancer

Thomas C. Harding *et al.*

Sci Transl Med **5**, 178ra39 (2013);
DOI: 10.1126/scitranslmed.3005414

Editor's Summary

Treating Cancer by Design

The Renaissance man (or woman) is held up as an ideal of someone with diverse knowledge. Yet, today, it is increasingly difficult to both be broad and have sufficient depth of knowledge to be successful in any one field. Unfortunately, this is also the case for cancer therapies. The most obvious outward signs of some cancers—severe weight loss, tiredness, hair loss, nausea—are actually caused by the nonspecific breadth of the treatments. One pathway that has proved particularly intractable is the fibroblast growth factor (FGF) pathway, which promotes tumor growth and angiogenesis but also contributes key metabolic hormones. Now, Harding *et al.* have designed a soluble FGF receptor Fc fusion protein (FP-1039) to overcome these difficulties.

The authors tested the specificity of FP-1039 both in vitro and in vivo across a wide swath of cancer types. FP-1039 binds to mitogenic FGF ligands, blocking angiogenesis and inhibiting growth of tumors of many different types. Tumors with amplified expression of, or mutations in, FGF receptors (such as certain lung and endometrial cancers) were especially well targeted by this drug. In contrast, FP-1039 did not bind tightly to the hormonal FGFs, and treatment in animal models had minimal toxicity. Although this drug has only been tested in early-stage clinical trial in humans, these data support a specialized inhibition of mitogenic FGFs. Cancer drug design is truly entering the Age of Reason.

Science Translational Medicine (print ISSN 1946-6234; online ISSN 1946-6242) is published weekly, except the last week in December, by the American Association for the Advancement of Science, 1200 New York Avenue NW, Washington, DC 20005.

CANCER

Blockade of Nonhormonal Fibroblast Growth Factors by FP-1039 Inhibits Growth of Multiple Types of Cancer

Thomas C. Harding, Li Long, Servando Palencia, Hongbing Zhang, Ali Sadra, Kevin Hestir, Namrata Patil, Anita Levin, Amy W. Hsu, Deborah Charych, Thomas Brennan, James Zanghi, Robert Halenbeck, Shannon A. Marshall, Minmin Qin, Stephen K. Doberstein, Diane Hollenbaugh, W. Michael Kavanaugh, Lewis T. Williams, Kevin P. Baker*

The fibroblast growth factor (FGF) pathway promotes tumor growth and angiogenesis in many solid tumors. Although there has long been interest in FGF pathway inhibitors, development has been complicated: An effective FGF inhibitor must block the activity of multiple mitogenic FGF ligands but must spare the metabolic hormone FGFs (FGF-19, FGF-21, and FGF-23) to avoid unacceptable toxicity. To achieve these design requirements, we engineered a soluble FGF receptor 1 Fc fusion protein, FP-1039. FP-1039 binds tightly to all of the mitogenic FGF ligands, inhibits FGF-stimulated cell proliferation in vitro, blocks FGF- and vascular endothelial growth factor (VEGF)–induced angiogenesis in vivo, and inhibits in vivo growth of a broad range of tumor types. FP-1039 antitumor response is positively correlated with RNA levels of *FGF2*, *FGF18*, *FGFR1c*, *FGFR3c*, and *ETV4*; models with genetic aberrations in the FGF pathway, including *FGFR1*-amplified lung cancer and *FGFR2*-mutated endometrial cancer, are particularly sensitive to FP-1039–mediated tumor inhibition. FP-1039 does not appreciably bind the hormonal FGFs, because these ligands require a cell surface co-receptor, klotho or β-klotho, for high-affinity binding and signaling. Serum calcium and phosphate levels, which are regulated by FGF-23, are not altered by administration of FP-1039. By selectively blocking nonhormonal FGFs, FP-1039 treatment confers antitumor efficacy without the toxicities associated with other FGF pathway inhibitors.

INTRODUCTION

Fibroblast growth factor (FGF)–FGF receptor (FGFR) signaling is a complex and redundant pathway comprising four receptors and 22 ligands, including the mitogenic FGFs (FGF-1 to FGF-10, FGF-16 to FGF-18, FGF-20, and FGF-22) and hormonal FGFs (FGF-19, FGF-21, and FGF-23). The FGFRs are activated by formation of a cell surface complex comprising two FGFRs, two FGF ligands, and heparin sulfate (*1*, *2*). The hormonal FGFs additionally require a membrane-anchored co-receptor, klotho or β-klotho, for high-affinity binding and signaling (*3*–*5*). FGFRs are tyrosine kinases that can phosphorylate signaling intermediates such as FRS2 and activate multiple signal transduction pathways including mitogen-activated protein kinase (MAPK)/extracellular signal–regulated kinase (ERK) and AKT. The FGF pathway regulates cell proliferation, metabolism, and survival, as well as plays instrumental roles in angiogenesis and tissue repair (*6*–*9*). FGFR signaling increases the mitotic rate of tumor cells, promotes tumor angiogenesis, and enhances tumorigenicity of cancer stem cells (*10*, *11*).

Mutation and overexpression of several FGFs and FGFRs, including activating mutations, chromosomal translocations, gene amplifications, and altered splicing patterns, are observed in cancer (*12*–*18*). Tumors with specific genetic alterations in the FGF pathway may be especially responsive to FGF inhibition. A recent survey of the genomic landscape of human cancer indicated that a highly focal region of DNA on chromosome 8 encompassing the *FGFR1* gene is frequently amplified in lung cancer tumors (*12*, *16*, *19*, *20*). In addition, somatic mutations in *FGFR2* are observed in 15 to 16% of endometrial carcinomas (*15*, *21*). The most common FGFR2 mutation is S252W (~7% of all cases), which is identical to the germline activating mutation in *FGFR2* seen in Apert syndrome, a congenital human skeletal disorder (*22*). Structure-function studies of FGFR2 S252W demonstrate that the mutant receptor has altered ligand specificity and enhanced affinity for multiple FGFs compared to wild-type FGFR2 (*23*).

Despite many years of research pointing to an important role for FGF signaling in cancer, the development of drugs specifically targeting the FGFR pathway has been difficult. A monoclonal antibody directed against the FGFR1 receptor failed because of severe weight loss associated with hypothalamic binding (*24*). Broad blockade of FGFR signaling using small molecules has also been associated with toxicity (*25*). In rats, treatment with PD176067, a small-molecule inhibitor of FGFR1 kinase activity, resulted in hyperphosphatemia and calcium-phosphorus deposition in various organs (*25*). In human clinical trials, the FGFR-specific inhibitors NVP-BGJ398 (Novartis) (*26*) and AZD4547 (AstraZeneca) (*27*) have caused increases in serum phosphate when administered to patients. These effects on phosphate metabolism are most likely on-target toxicities caused by inhibition of FGF-23 signaling (*25*). FGF-23, a hormone originally identified as the cause of hypophosphatemic rickets (*28*), reduces phosphate and calcium levels in the blood by acting on sodium-phosphate cotransporters in the kidney (*29*).

To achieve blockade of the mitogenic FGFs while avoiding inhibition of hormonal FGFs, we developed a soluble decoy receptor, FP-1039. The FGFR1c isoform (FGFR1 containing the c-splice region in domain III) (*30*) was chosen because it has a broad FGF ligand–binding profile (*31*) and does not bind the hormonal FGFs with high affinity in the absence of klotho or β-klotho (*3*, *32*). Consistent with these findings, FP-1039 binds to and inhibits the mitogenic members of the FGF family but exhibits little or no affinity for the hormonal FGFs. FP-1039 inhibits angiogenesis and the FGF/FGFR autocrine growth loops that drive tumor cell proliferation. Preclinical cancer models with genetic aberrations in the FGF pathway, including *FGFR1*-amplified lung cancer and *FGFR2*-mutated endometrial cancer, are particularly sensitive to FP-1039–mediated tumor inhibition.

Five Prime Therapeutics Inc., 2 Corporate Drive, South San Francisco, CA 94080–7047, USA.
*Corresponding author. E-mail: kevin.baker@fiveprime.com

RESULTS

Design and initial characterization of FP-1039

The extracellular domain (ECD) of the FGFR1c isoform was coupled to the Fc domain of immunoglobulin G1 (IgG1) to create a trap for FGF ligands (Fig. 1A). Surface plasmon resonance (SPR) spectroscopy (Table 1) shows that FP-1039 binds to FGF-1, FGF-2, FGF-4, FGF-6, FGF-8b, FGF-9, FGF-16, FGF-17, and FGF-18 with high affinity [dissociation constant (K_d), $<10^{-10}$ M], to FGF-3, FGF-5, and FGF-20 with moderate affinity (K_d, 1×10^{-9} to 7×10^{-9} M), and to FGF-23 with low affinity (K_d, 3.28×10^{-8} M). There was no measurable binding to FGF-7, FGF-10, FGF-12, FGF-19, FGF-21, and FGF-22. FP-1039 also binds to FGF ligands from other species: Its affinity for FGF-1, FGF-2, and FGF-4 is similar for human and rat proteins. FP-1039 does not bind to other classes of growth factors including epidermal growth factor (EGF), platelet-derived growth factor (PDGF), and vascular endothelial growth factor (VEGF).

FP-1039 inhibited FGF-2–induced ERK phosphorylation in L6 cells modified to overexpress FGFR1 with a median inhibitory concentration (IC_{50}) value of 0.023 μg/ml (Fig. 1B) and blocked FGF-2–stimulated A549 cell proliferation with an IC_{50} of 0.01 μg/ml (Fig. 1C).

Inhibition of VEGF- and FGF-induced angiogenesis by FP-1039

Administration of FP-1039 (5 mg/kg or higher) completely blocked in vivo angiogenesis induced by a Matrigel plug impregnated with FGF-2 (Fig. 1D and fig. S1). Administration of FP-1039 (15 or 45 mg/kg) also completely blocked in vivo angiogenesis in response to a Matrigel plug impregnated with VEGF-A only or FGF-2 plus VEGF-A (fig. S1). Antiangiogenic activity against VEGF-induced angiogenesis in this model system likely reflects inhibition of the synergistic activity between VEGF in the plug and murine-derived stromal FGFs because SPR analysis shows that FP-1039 does not directly interact with VEGF-A. Likewise, FP-1039 does not block VEGF-induced proliferation of human umbilical vein endothelial cells (HUVECs), although it is capable of blocking FGF-induced HUVEC proliferation (fig. S2).

Antitumor activity of FP-1039 in xenograft models

The antitumor activity of FP-1039 was evaluated in a panel of 35 xenograft models (table S1). In addition to standard cell line–derived tumor models, five patient-derived xenograft (PDX) lung cancer models (tables S1 and S2) were also examined in which human tumor fragments are expanded solely within mice rather than cell culture (*33*). In responding tumors, FP-1039 significantly reduced tumor volume as assessed by area under the curve analysis. Responses were observed in 19 of 35 (54%) of the models examined, with a range of 25 to 96% inhibition (table S1). Representative tumor growth curves are presented in Fig. 2. In the renal cell carcinoma (RCC) Caki-1 model, administration of FP-1039 at 10 mg/kg twice a week for 6 weeks resulted in 81% ($P < 0.001$) tumor growth inhibition (TGI; Fig. 2A). In the MSTO-211H mesothelioma model, FP-1039 administration reduced tumor growth (Fig. 2B) by 64% ($P < 0.0001$). No additional antitumor activity was observed above the dose level of 15 mg/kg. Antiangiogenic activity was observed directly in the Caki-1 tumor xenografts by staining for CD31; following treatment with FP-1039 (fig. S3) reduced CD31 staining is observed.

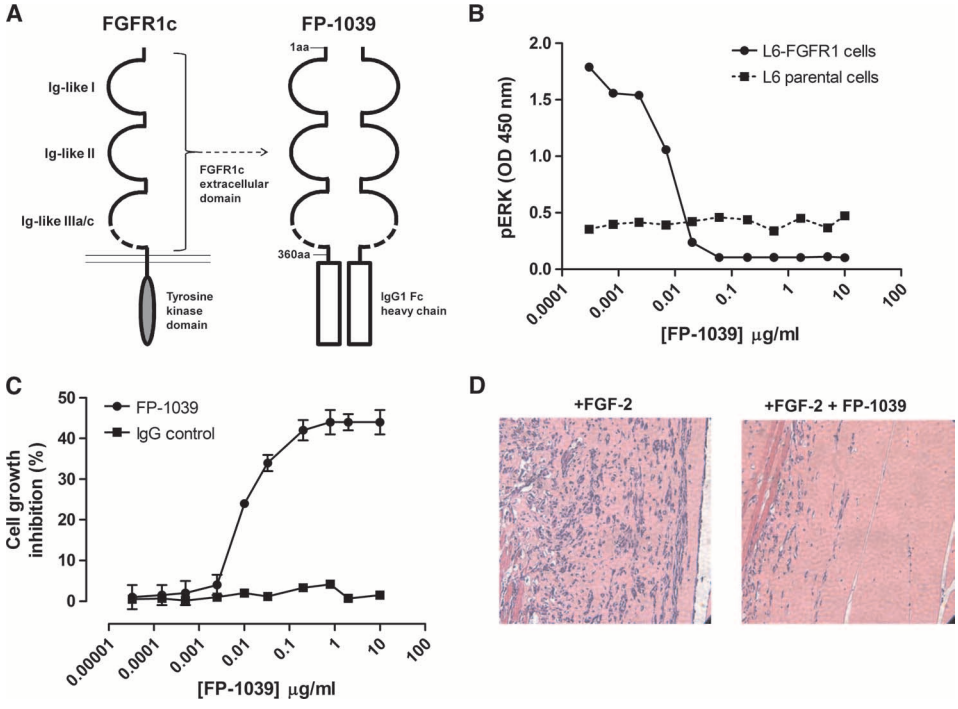

Fig. 1. Design and preliminary analysis of FP-1039. (**A**) Schematic diagram of FP-1039. A soluble FGFR1 receptor was constructed by addition of the human IgG1 Fc region to the extracellular ligand-binding domain of FGFR1c receptor splice isoform. (**B**) Inhibition of FGF-2–induced ERK phosphorylation by FP-1039 in L6 cells overexpressing human FGFR1c. OD, optical density. (**C**) FP-1039–mediated inhibition of FGF-2–stimulated A549 cell proliferation. The percentage of inhibition was determined by comparison to proliferation in the presence and absence of FGF-2 alone. IC_{50} represents the concentration of soluble receptor required for half-maximal inhibition. (**D**) Inhibition of FGF-2–induced angiogenesis in vivo by FP-1039 as determined by the Matrigel plug assay.

Inhibition of FGFR1 signaling by FP-1039 in vivo

Inhibition of FGFR1 signaling by FP-1039 was examined in vivo in the JIMT-1 xenograft model by preparing tumor lysates 24 and 72 hours after dose and measuring levels of phosphorylated FGFR1, FRS2, and AKT (fig. S4). FP-1039 reduced levels of phosphorylated FGFR1 by 24 hours after dose and completely abolished FGFR1 phosphorylation by 72 hours after dose. Phosphorylated FRS and AKT levels were reduced 24 hours after dose and further reduced 2 days later.

Preclinical efficacy of FP-1039 in an endometrial model with FGFR2 mutation

We examined the in vivo sensitivity of FGFR2 S252W bearing mutant (MFE-280) and wild-type (HEC-1-B) human endometrial carcinoma cell lines to FP-1039. FP-1039 treatment of mice bearing HEC-1-B xenografts resulted in a 30% ($P < 0.01$) TGI (table S1). In comparison, FP-1039

Table 1. FGF ligand–binding profile of FP-1039 as determined by Biacore.

Ligand	Affinity to FP-1039 (M)*
FGF-1	3.10×10^{-11}
FGF-2	4.62×10^{-10}
FGF-3	2.92×10^{-9}
FGF-4	6.75×10^{-10}
FGF-5	2.95×10^{-9}
FGF-6	3.40×10^{-10}
FGF-7	0
FGF-8b	4.56×10^{-10}
FGF-9	9.19×10^{-10}
FGF-10	0
FGF-12	0
FGF-16	4.04×10^{-10}
FGF-17	5.94×10^{-10}
FGF-18	2.99×10^{-10}
FGF-19	0
FGF-20	1.51×10^{-9}
FGF-21	0
FGF-22	0
FGF-23	6.70×10^{-8}

*FP-1039 ligand-binding affinity was determined in the presence of heparin sulfate (50 μg/ml).

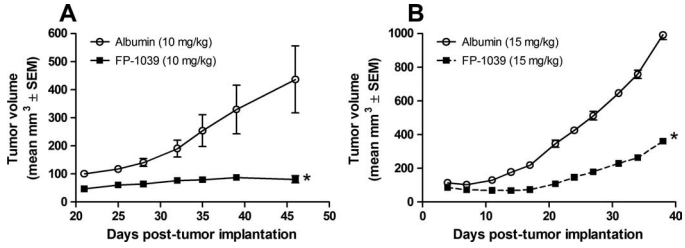

Fig. 2. Antitumor activity of FP-1039 in selected xenograft models. (**A** and **B**) Efficacy of FP-1039 in a renal cancer, Caki-1 (A), and mesothelioma, MSTO-211H (B), xenograft cancer model. Five million cells were implanted subcutaneously over the right flank of severe combined immunodeficient (SCID) mice (n = 10 per group). FP-1039 or albumin was administered intraperitoneally twice a week at a dose of 10 or 15 mg/kg, Caki-1 and MSTO-211H, respectively. *P < 0.05.

administration in the MFE-280 xenograft model yielded 95% TGI (P < 0.001) when compared to vehicle-treated controls (Fig. 3A).

Antitumor activity of FP-1039 in lung cancer models with FGFR1 genomic amplification

We identified five lung cancer cell lines that displayed genomic *FGFR1* gene amplification on chromosome 8. Small cell lung cancer (SCLC) lines DMS53 and DMS114 contained 5 and 10 copies per cell, respectively, of the *FGFR1* gene. Three non-SCLC (NSCLC) lines—NCI-H1581, NCI-H520, and NCI-H1703—had six, eight, and six copies, respectively. FP-1039 inhibited growth of each of the five cell lines in vitro (figs. S5 and S6).

FP-1039 inhibited growth of subcutaneous xenografts generated from each of the five cell lines (Fig. 3, B to D). The degree of TGI by FP-1039 for DMS114, DMS53, NCI-H1581, NCI-H520, and NCI-H1703 was 64, 64, 74, 47, and 31%, respectively. The NCI-H1703 cell line (31% TGI) contains a drug-sensitive *PDGFRA*/*PDGFC* genomic amplification in addition to *FGFR1* amplification (*34*, *35*), possibly explaining the modest efficacy observed for FP-1039 in this model.

Lung cancer xenografts with *FGFR1* gene amplification had an average 56% TGI with FP-1039 treatment versus control (Fig. 3D). In comparison, lung cancer xenografts without *FGFR1* gene amplification displayed an average 22% TGI. The difference in FP-1039–mediated xenograft inhibition between *FGFR1* gene–amplified and nonamplified lung cancer xenograft models was statistically significant (P = 0.0333). Note, however, that *FGFR1* gene amplification is not the sole determinator of FP-1039 antitumor effect because lung xenograft models with a normal, diploid copy number of *FGFR1* can have a significant response to FP-1039, comparable to lung models with *FGFR1* amplification (Fig. 3D).

In these experiments, FP-1039 reduced tumor growth but did not cause tumor regression (table S2). It is possible that in these xenograft models, trapping of the ligands alone may not be sufficient to completely shut down these pathways. Previous studies of small-molecule FGFR tyrosine kinase inhibitors (*16*) caused regression of tumor xenograft possibly because the inhibitors block ligand-independent FGFR activity or because they block additional kinases such as the VEGF receptor KDR.

The efficacy of FP-1039 was also examined in preclinical models in combination with standard-of-care chemotherapy regimens for broad cancer indications. In an SCLC DMS53 (*FGFR1* gene–amplified) model, FP-1039 efficacy was examined in combination with cisplatin and etoposide (Fig. 4). Addition of FP-1039 to the cisplatin/etoposide combination resulted in an additional decrease in DMS53 tumor growth, which was statistically significant compared to all other groups (P < 0.001).

Identification of molecular markers predictive of preclinical FP-1039 efficacy

To further understand the potential molecular determinants that make xenograft models (n = 35; table S1) sensitive to treatment with FP-1039, we examined the RNA expression of a panel of FP-1039–related genes including FGF ligands, FGFRs, FGF-binding proteins, and FGF signaling molecules using quantitative reverse transcription polymerase chain reaction (qRT-PCR) (table S3). Gene expression was then correlated to FP-1039 response to determine RNA expression signatures positively and negatively correlated with antitumor impact (Table 2 and table S4). Expression of *FGFR1* (P = 0.01669; Fig. 5A), specifically the *FGFR1c* splice variant (P = 0.0431), was positively correlated with FP-1039 antitumor activity. Expression of the *FGFR1b* splice variant was not correlated with FP-1039 response (table S4). In addition to *FGFR1*, expression of the *FGFR3c* receptor (P = 0.01944) was also positively correlated with FP-1039 antitumor response (Fig. 5B), reflecting the broad overlap in FGF ligand–binding specificity between the c-splice isoforms of FGFR1 and FGFR3 receptors (*31*, *36*).

Expression of *FGF2* (P = 0.03569) was positively associated with FP-1039 response (Fig. 5C). Of all the gene expression targets

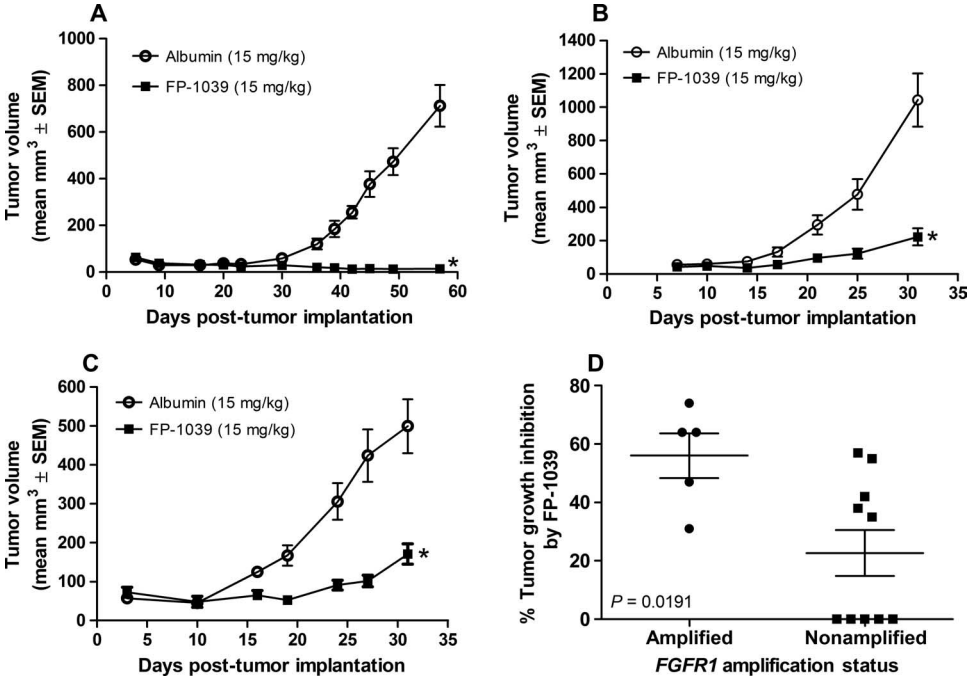

Fig. 3. FP-1039 inhibits tumor growth in endometrial and lung cancer models with genetic aberrations in FGFR1 or FGFR2. (**A**) Efficacy of FP-1039 in the *FGFR2*-mutated (S252W) endometrial cancer model MFE-280. Five million MFE-280 cells were implanted subcutaneously over the right flank of SCID mice (n = 10 per group). FP-1039 or albumin was administered intraperitoneally twice a week at a dose of 15 mg/kg. *P < 0.01. (**B** and **C**) Efficacy of FP-1039 in the *FGFR1* gene–amplified NCI-H1581 NSCLC model (B) and DMS114 SCLC (SCLC) model (C). Five million NCI-H1581 or DMS114 cells were implanted subcutaneously over the right flank of SCID mice (n = 10 per group). FP-1039 or albumin was administered intraperitoneally twice a week at a dose of 15 mg/kg. *P < 0.01. (**D**) Comparison of FP-1039–mediated TGI in *FGFR1*-amplified (n = 5) and nonamplified (n = 10) lung cancer models. Lung xenograft models without *FGFR1* amplification examined in this experiment were as follows: A549, NCI-H460, NCI-H226, NCI-H2126, NCI-H441, NCI-H358, NCI-H522, Calu-1, D35087, and D37638.

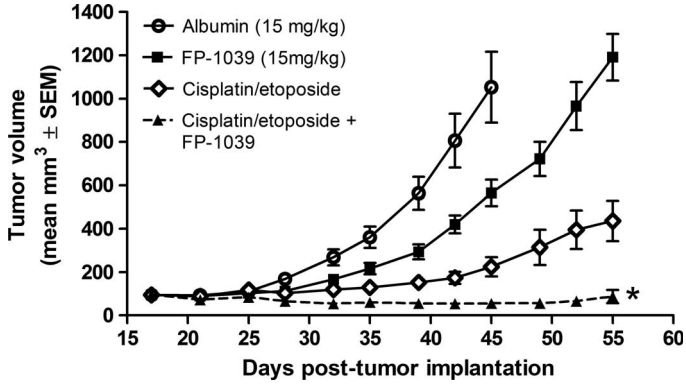

Fig. 4. Combination of FP-1039 with cisplatin and etoposide in the DMS53 SCLC xenograft model. Five million DMS53 cells were implanted subcutaneously over the right flank of SCID mice (n = 10 per group). FP-1039 or albumin was administered intraperitoneally at 15 mg/kg twice per week starting on day 17 after tumor implantation when the average tumor volume reached 100 mm^3. Cisplatin was administered intraperitoneally at 3 mg/kg once per week starting on day 17 after tumor implantation. Etoposide was administered intraperitoneally at 4 mg/kg daily for three consecutive days per week starting at day 17 after tumor implantation. *P < 0.01 comparing cisplatin + etoposide to cisplatin + etoposide + FP-1039.

examined, *FGF2* displayed the highest ratio (247.7-fold) of median gene expression between FP-1039 responder and nonresponder xenograft models. The association of *FGF2* with FP-1039 efficacy in xenograft models was confirmed at the protein level using tumor lysates (Fig. 5D). In addition to *FGF2*, RNA expression of the *FGF18* ligand (P = 0.02227) was also positively (6.9-fold) correlated with FP-1039 antitumor activity. The downstream target gene of FGF signaling, ets variant 4 (*ETV4*), was the most significant (P = 0.01639) gene for its positive (2.897-fold) association with FP-1039 activity. Significant genes with a negative association with FP-1039 activity were not found in this analysis.

To determine what RNA markers may determine lung xenograft response in the absence of *FGFR1* gene amplification (Fig. 3D), we analyzed the correlation of FP-1039 response in the non–*FGFR1*-amplified subset of lung models (n = 13; table S5). Results indicated that *FGF2* expression was the only significant (P = 0.029) gene up-regulated >3000-fold in responding versus nonresponding *FGFR1* nonamplified lung models. The expression of *FGFR1c* and *FGFR3c* did display a positive trend with FP-1039 response in the non–*FGFR1*-amplified lung subset; however, this did not reach statistical significance in these experiments.

We next examined if there was a correlation in gene expression among the significant gene markers identified for their association with FP-1039 response (Table 2) in all models. Results from this analysis (table S6) indicate that there is a significant, positive correlation between most of the individual RNA markers identified as predictive for FP-1039 xenograft response. For example, xenograft *FGF2* RNA expression is positively correlated with *FGFR3c*, *FGFR1c*, and *FGFR1* expression (P < 0.05); *FGFR1* RNA expression is positively correlated with *FGFR3c*, *FGF2*, and *FGF18*. The expression of *ETV4* was the only gene identified for which a significant association with other FP-1039–responsive genes was not identified.

FP-1039 has no impact on serum phosphate levels in rats

FP-1039 binds to the mitogenic FGFs with 10- to 100-fold higher affinity than to FGF-23 (Table 1). The binding affinity of FP-1039 for rodent FGF-23 is comparable to that of human FGF-23 by SPR analysis (6.0×10^{-8} M versus 6.7×10^{-8} M). We investigated the potential biological impact of this relatively weak FP-1039/FGF-23 binding in rats after four weekly doses of FP-1039 at a dose range of 10 to 200 mg/kg twice per week. Plasma exposure of the drug was confirmed by an ELISA that measures free drug (Fig. 6A). At a dose of 200 mg/kg twice per week, the maximal plasma concentration of the drug was 3.6 and 4.2 mg/ml for female and male rats, respectively. Despite these sustained high levels of the drug, no significant changes in plasma phosphate were

observed for any FP-1039 dose compared to animals that received vehicle [9.61 mg/dl versus 10.19 mg/dl for vehicle and FP-1039 (200 mg/kg twice per week), respectively]. In contrast, daily dosing of rats with the small-molecule FGFR kinase inhibitor PD173043 resulted in significantly elevated plasma phosphate levels at either 24 hours or 1 week of daily dosing (Fig. 6B). Additionally, histological analysis of 55 tissues in animals treated with high-dose FP-1039 failed to reveal any changes consistent with those reported by Brown *et al.* (*25*), who observed hyperphosphatemia and calcium-phosphorus deposition in various organs after administration of a small-molecule inhibitor of FGFR1 kinase activity. In addition, FP-1039 has completed a phase 1 dose-escalation study (n = 39) of up to 16 mg/kg twice per week in patients with solid tumors. No impact of FP-1039 on serum phosphate was observed at any of the dose levels examined (*37*). In summary, these in vivo data support the biophysical data that FP-1039 does not bind to FGF-23 with high affinity and does not induce hyperphosphatemia as was shown for other broad inhibitors of the FGFR pathway.

Table 2. RNA levels of FGF ligands and receptors correlated with FP-1039 efficacy in xenograft models.

Gene	Ratio*	P†
ETV4	2.897	0.01639
FGFR1	2.447	0.01669
FGFR3c	9.863	0.01944
FGF18	6.915	0.02227
FGF2	247.7	0.03569
FGFR1c	3.647	0.0431

*Gene expression ratio was determined by median gene expression in FP-1039 responders/median gene expression in nonresponders. †*P* value was determined by Mann-Whitney.

DISCUSSION

FP-1039 has two distinct mechanisms of action: it inhibits tumor cell proliferation (Fig. 1C and figs. S5 and S6) and blocks angiogenesis (Fig. 1D and figs. S1 to S3). FP-1039 inhibits both VEGF-A– and FGF-2–induced angiogenesis in the Matrigel plug model, consistent with findings that both FGF and VEGF signaling are required in concert for vessel growth in vivo (*38*). The impact of FP-1039 on VEGF-A–induced angiogenesis appears to be indirect requiring the in vivo environment, because (i) FP-1039 does not bind VEGF-A directly as determined by SPR analysis and (ii) no in vitro activity of FP-1039 was observed against VEGF-A in a HUVEC proliferation assay (fig. S2). Experimentally, synergy of VEGF and FGF-2 in the angiogenic process has previously been demonstrated (*38*, *39*). Despite observing inhibition of VEGF-induced angiogenesis in preclinical models, no clinical toxicities consistent with VEGF inhibition were observed in a completed phase 1 clinical trial of FP-1039 including proteinuria or hypertension (manuscript in preparation).

The tumor expression of *FGFR1*, specifically the c "mesenchymal" splice isoform *FGFR1c*, which forms the extracellular ligand-binding domain of FP-1039, positively correlates with response in xenograft models. In addition, the expression of *FGFR3c*, which binds several ligands that bind FP-1039 (*36*), and the expression of *FGF18* and *FGF2* RNA and protein also positively correlate with FP-1039 response. The association of FP-1039 response and FGF-2 expression in vitro has previously been reported in head and neck squamous cell carcinoma cell lines by Marshall and colleagues (*40*). We also found that the expression of *ETV4*, a downstream target gene of FGF signaling, was positively associated with FP-1039 response.

The *FGFR1* gene is frequently amplified in lung cancer tumors (*12*, *16*, *19*, *20*). Subtype analysis indicates that *FGFR1* gene amplification is observed in about 22% of squamous NSCLCs and 6% of SCLCs (*16*, *19*, *20*). Preliminary data also support the existence of *FGFR1* amplification in about 10% of pulmonary pleomorphic carcinomas (*41*). Amplification of the *FGFR1* gene in lung cancer cell lines is associated with overexpression of the FGFR1 protein and increased signaling through the FGFR1 pathway,

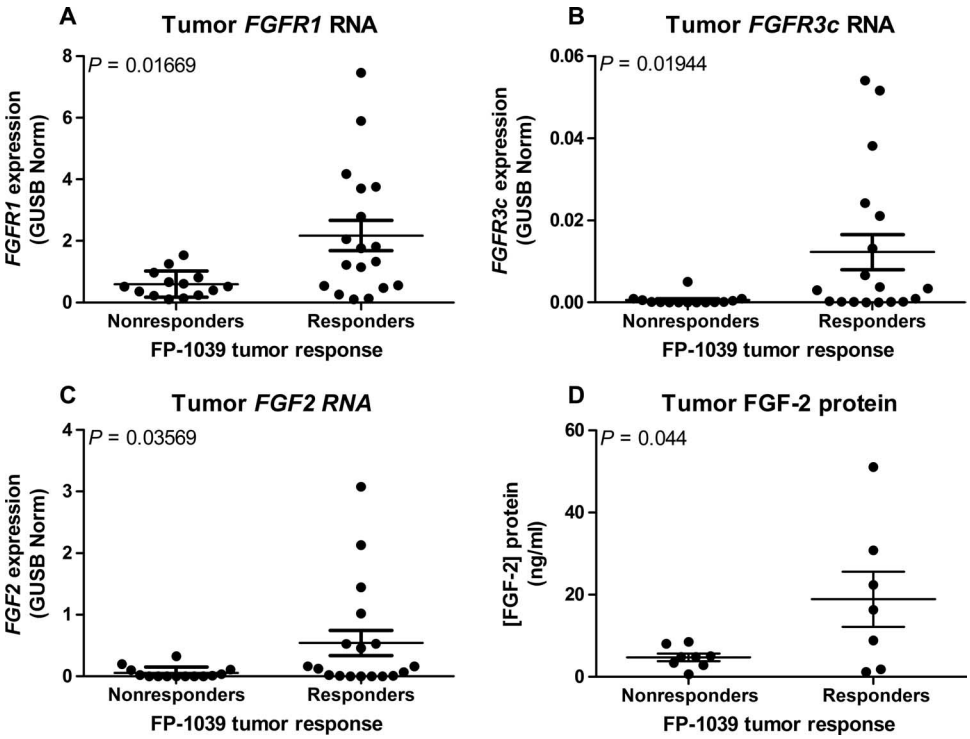

Fig. 5. FGF ligands and receptors correlated with FP-1039 antitumor efficacy. (**A** to **C**) Tumor *FGFR1* (A), *FGFR3c* (B), and *FGF2* (C) gene expression was determined with qRT-PCR in FP-1039–responsive and nonresponsive xenograft models. (**D**) Tumor FGF-2 protein levels were determined by enzyme-linked immunosorbent assay (ELISA) and compared between FP-1039–responsive and nonresponsive xenografts models.

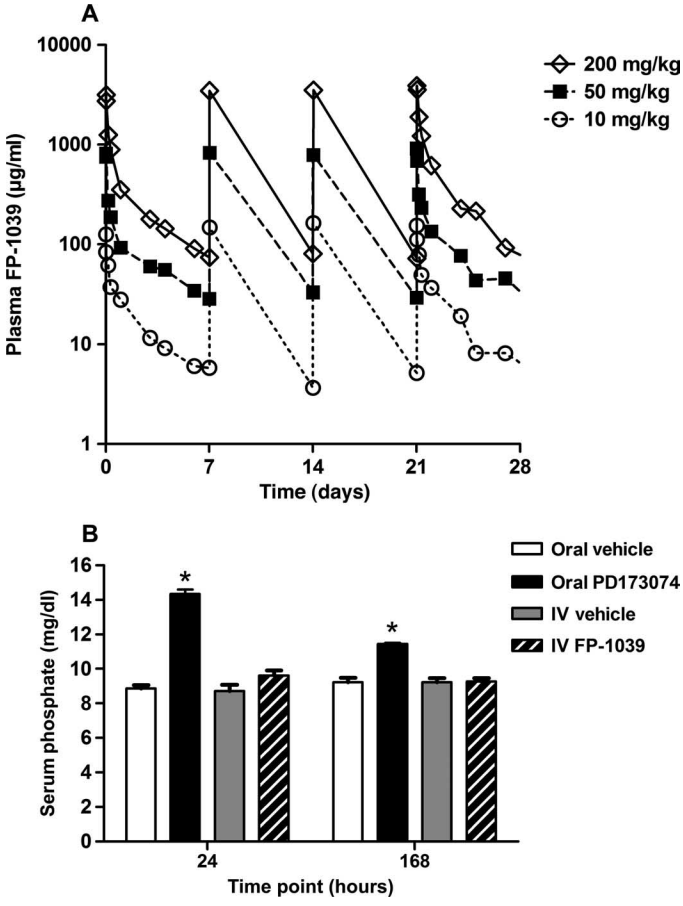

Fig. 6. FP-1039 does not alter plasma phosphate homeostasis in rats. (**A**) Plasma concentrations of drug in rats administered FP-1039. Animals (n = 5 per group) were dosed with vehicle and FP-1039 (10, 50, or 200 mg/kg twice per week) for four weekly doses, and plasma concentrations of FP-1039 were determined throughout the study by an ELISA-based detection method. (**B**) Female Sprague-Dawley rats were administered the FGFR kinase inhibitor PD173074 or vehicle control by oral gavage daily for 7 days or FP-1039 and appropriate vehicle by intravenous (IV) administration. Serum phosphate levels were determined at 24 and 168 hours after initiation of dosing. *P < 0.05 comparing oral PD173074 to vehicle groups.

resulting in enhanced cell proliferation and resistance to apoptosis (*16*, *20*). Cell lines with *FGFR1* amplification are highly sensitive to RNA interference–mediated down-regulation of FGFR1 expression and small-molecule FGFR inhibitors (*16*, *20*). It has been suggested that amplification of *FGFR1* may result in a ligand-independent activation (*16*, *42*). The sensitivity to FP-1039, a ligand trap, demonstrated in this report suggests that many tumors containing *FGFR1* amplifications remain responsive to FGF ligands and therefore represent good targets for therapy with FP-1039.

MATERIALS AND METHODS

Construction and expression of FP-1039

FP-1039 fusion protein was constructed by linking the complementary DNA (cDNA) encoding the ECD of human FGFR1c to the cDNA encoding the hinge and Fc domain of human IgG1 with standard molecular biology techniques. The fusion cDNA construct was inserted into a CHEF1 expression vector (*43*) and used to stably transfect Chinese hamster ovary (CHO) cells. Stable cell clones were selected for high-level FP-1039 production and grown to large volume in suspension. FP-1039 protein expressed from recombinant host cells was purified to homogeneity from cell culture supernatant with sequential protein A affinity, ion exchange, and hydrophobic interaction chromatography.

SPR studies of FP-1039 FGF-binding affinity

The specificity of FGF ligand binding to FP-1039 was assessed by SPR with a Biacore T100. Protein A or anti-human IgG antibody (Biacore) was covalently linked to a CM5 chip by amine coupling. FP-1039 protein was captured, and FGF ligands were flowed over the FGFR fusion protein in the presence of HBS-P running buffer (Biacore) supplemented with heparin sulfate (50 μg/ml) (Sigma). All the recombinant FGF ligands were from R&D Systems and PeproTech, except for FGF-18, which was from Wako Chemicals. FGF ligands were each tested at six to eight concentrations ranging from 4.5 ng/ml to 10 μg/ml. The FGF ligands were of human origin, except for FGF-8b and FGF-18, which were of recombinant mouse origin.

Matrigel plug assay

Recombinant human FGF-2 (final concentration, 250 ng/ml; PeproTech) and/or recombinant human VEGF-A (final concentration, 100 ng/ml; PeproTech) were added to Matrigel (BD Biosciences) with sodium heparin (2 U/ml; Sigma). FGF-2 and/or VEGF-A containing Matrigel plugs (one per animal) were implanted subcutaneously in the abdomen region of C57BL/6 mice (Charles River Laboratories). FP-1039 was administered by tail vein injection on days 1, 4, and 7 after Matrigel implantation. On day 9, plugs were excised and processed for hematoxylin and eosin staining. Digital images of the stained Matrigel sections were generated with a Retiga-2000R digital camera (QImaging). Image analysis was performed with Image-Pro Plus 5.1 (Media Cybernetics Inc.). Neovascularization was defined as the cellular response in the Matrigel plugs, consisting of newly formed blood vessels and migrated cells.

Cells

Cell lines were obtained from the Health Protection Agency, German Collection of Microorganisms and Cell Cultures, and American Type Culture Collection and cultured according to the vendors' instructions. A panel of lung cancer cell lines displaying potential amplification of the *FGFR1* gene was identified with CONAN (http://www.sanger.ac.uk/cgi-bin/genetics/CGP/conan/search.cgi) and Tumorscape (http://www.broadinstitute.org/tumorscape/pages/portalHome.jsf).

FGFR1 amplification assay

Amplification status of the *FGFR1* gene in the cell lines was determined by QuantiGene Plex DNA Assay (Panomics/Affymetrix). Individual, bead-based, oligonucleotide probe sets (including capture, capture extenders, blockers, and label probes) specific for *FGFR1* (NM_023110), *ALB* (NM_000477), and *DCK* (NM_000788) genes were designed to prevent cross-reactivity and synthesized by Panomics. *ALB* and *DCK* were used as reference genes for normalizing *FGFR1* copy number. Cells were lysed to release DNA and incubated overnight with gene-specific capture bead probe sets. The beads and bound target DNAs were washed and subsequently incubated with amplifier reagents,

followed by biotinylated label probes and finally streptavidin-conjugated R-phycoerythrin (SAPE), with thorough washing in between each step. SAPE fluorescence was detected at 575 nm for each capture bead with a Luminex 200 flow cytometer instrument (Luminex). All data were normalized to the reference genes and expressed as a ratio (*FGFR1/ALB*).

FGF-2–stimulated phospho-ERK assay

Rat skeletal muscle L6 cells transfected with FGFR1c (ETR) were seeded in a 96-well flat-bottomed plate (Becton Dickinson) at 1×10^4 cells per well in Dulbecco's modified Eagle's medium (DMEM) supplemented with 0.5% fetal bovine serum (FBS) and 0.1% bovine serum albumin (BSA) and incubated for 16 hours. Activation medium containing FP-1039 or human IgG1, at concentrations from 0 to 10 μg/ml, was prepared [in 0.1% BSA/DMEM containing FGF-2 (100 ng/ml) and heparin (10 μg/ml)] and incubated for 30 min at 37°C on a plate shaker. The L6-FGFR1c cells were then exposed to 25 μl of activation medium per well for 5 min at 37°C. The cells were then washed and lysed, and cell lysate phospho-ERK levels were determined with the PathScan Phospho-p44/42 MAPK Sandwich ELISA Kit (Cell Signaling) following the manufacturer's instructions.

FGF-2–stimulated cell proliferation assay

Human lung adenocarcinoma A549 cells were plated in a Microtest 96-well tissue culture plate (Becton Dickinson) at a density of 5×10^3 cells per well in F-12K medium supplemented with 0.1% FBS, FGF-2 (10 ng/ml), and heparin (10 μg/ml) in the presence of varying concentrations of FP-1039 or an unrelated ECD-Fc negative control. Plates were incubated at 37°C at 5% CO_2 for 4 days and then assayed with the CellTiter-Glo Luminescent Cell Viability Assay (Promega). Luminescence was determined on an EnVision Multilabel Plate Reader (PerkinElmer) with a 0.2-s integration time. Results were expressed as relative light units per well.

Quantification of FP-1039 by ELISA

FP-1039 concentration in plasma was determined with a quantitative ELISA. Briefly, recombinant human FGF-2 (R&D Systems) was immobilized on a half-well microtiter ELISA plate, blocked, and incubated with test samples [diluted 1:10 with blocking buffer/heparin (20 μg/ml)]. The plate was subsequently washed, and a dilute goat anti-human IgG-Fc horseradish peroxidase antibody solution (Sigma) was added and incubated. After a final wash step, a tetramethylbenzidine peroxidase substrate solution was added and incubated at ambient temperature with gentle shaking. The reaction was stopped with a phosphoric acid solution. Plates were read on a plate reader (450 nm). FP-1039 concentrations were determined on a standard curve obtained by plotting optical density versus concentration.

Efficacy studies in tumor xenograft models

All in vivo work was conducted under appropriate Institutional Animal Care and Use Committee–approved protocols. Six- to 8-week-old female SCID mice were obtained from Charles River Laboratories and housed under specific pathogen–free conditions. For subcutaneous tumor models, 5×10^6 tumor cells were resuspended in 50 μl of sterile phosphate-buffered saline, mixed 1:1 (v/v) with Matrigel (BD Biosciences), and injected subcutaneously into the right dorsal flank. For studies in PDX models (table S1), tissue fragments were obtained from primary tumor samples serially passaged in donor SCID mice and cut into 1- to 2-mm-diameter fragments (~25 mg). Recipient mice were anaesthetized by isoflurane inhalation, a small pocket was formed with blunt forceps, one fragment of tumor PDX was placed in the pocket, and the wound was sealed. In all studies, unless indicated, FP-1039, vehicle control, or a negative control human IgG1 antibody was each administered intravenously or intraperitoneally twice weekly. The length of treatment was determined based on the growth kinetics of each tumor model. Study endpoints included tumor growth and body weight observation. Tumor volume was calculated in cubic millimeters (volume = length × width^2 × 0.5). Mice were euthanized and recorded as a "conditional death" when the tumor volume exceeded 2000 mm^3 or when the tumors became excessively necrotic. The mean tumor volume in the treatment group(s) versus control group was compared with either Student's *t* test for studies with only two groups or analysis of variance (ANOVA) followed by Tukey's test for studies with more than two groups. Data are presented as means ± SEM.

Impact of PD173074 and FP-1039 on serum phosphate in rats

Sprague-Dawley rats (Charles River Laboratories; $n = 5$ per group) were administered the FGFR kinase inhibitor PD173074 (Chemdea; 50 mg/kg per day) or vehicle control by oral gavage for 7 days. In separate experimental arms, FP-1039 (200 mg/kg) or appropriate vehicle was dosed weekly by intravenous administration. Blood samples were collected at the time points indicated, and serum phosphate was determined (IDEXX Laboratories).

qRT-PCR analysis of xenograft RNA expression

RNA was extracted from cell lines grown in vitro or tumor xenografts grown in vivo with the RNeasy Mini kit (Qiagen). Extracted RNA was treated with deoxyribonuclease I before creating cDNA with random hexamer priming and reverse transcriptase using the QuantiTect Reverse Transcription Kit (Qiagen). Human and mouse RNA expression was determined using QuantiTect Primer Assays (Qiagen) with a human *GUSB* control reference QuantiTect Primer Assay (Qiagen). QuantiTect SYBR Green PCR Kits (Qiagen) were used to quantify mRNA expression levels with real-time qRT-PCR and an ABI Prism ViiA 7 Real-Time PCR System (Applied Biosystems). Relative gene expression quantification was calculated according to the comparative C_t method with human GUSB as a reference and commercial RNA controls (Stratagene). Relative quantification was determined according to the following formula: $2^{-(\Delta Ct\ \text{sample} - \Delta Ct\ \text{calibrator})}$.

SUPPLEMENTARY MATERIALS

www.sciencetranslationalmedicine.org/cgi/content/full/5/178/178ra39/DC1

Fig. S1. FP-1039–mediated inhibition of FGF-2– and VEGF-A–induced angiogenesis in the Matrigel plug assay.

Fig. S2. FP-1039 does not inhibit VEGF-A–induced HUVEC proliferation.

Fig. S3. FP-1039 inhibits tumor angiogenesis in the Caki-1 RCC xenograft model.

Fig. S4. FP-1039–mediated inhibition of FGFR1 signaling in the JIMT-1 breast cancer xenograft model.

Fig. S5. Lung cancer cell lines with *FGFR1* gene amplification are inhibited by FP-1039 in vitro as assessed by CellTiter-Glo Luminescent Cell Viability Assay.

Fig. S6. Lung cancer cell lines with *FGFR1* gene amplification are inhibited by FP-1039 in vitro as assessed by tritiated thymidine incorporation assay.

Table S1. Summary of FP-1039 antitumor activity in a panel of xenograft models.

Table S2. Characteristics of lung cancer PDX models.

Table S3. qRT-PCR gene expression data for xenograft models.

Table S4. Statistical analysis of FGF-related gene expression in relation to FP-1039 antitumor response in xenograft models.
Table S5. Statistical analysis of FGF-related gene expression in relation to FP-1039 antitumor response in non–*FGFR1*-amplified lung xenograft models.
Table S6. Spearman correlation of gene expression markers predictive of FP-1039 efficacy in xenograft models.

REFERENCES AND NOTES

1. L. Pellegrini, D. F. Burke, F. von Delft, B. Mulloy, T. L. Blundell, Crystal structure of fibroblast growth factor receptor ectodomain bound to ligand and heparin. *Nature* **407**, 1029–1034 (2000).
2. N. J. Harmer, L. L. Ilag, B. Mulloy, L. Pellegrini, C. V. Robinson, T. L. Blundell, Towards a resolution of the stoichiometry of the fibroblast growth factor (FGF)–FGF receptor–heparin complex. *J. Mol. Biol.* **339**, 821–834 (2004).
3. H. Kurosu, Y. Ogawa, M. Miyoshi, M. Yamamoto, A. Nandi, K. P. Rosenblatt, M. G. Baum, S. Schiavi, M. C. Hu, O. W. Moe, M. Kuro-o, Regulation of fibroblast growth factor-23 signaling by klotho. *J. Biol. Chem.* **281**, 6120–6123 (2006).
4. H. Kurosu, M. Choi, Y. Ogawa, A. S. Dickson, R. Goetz, A. V. Eliseenkova, M. Mohammadi, K. P. Rosenblatt, S. A. Kliewer, M. Kuro-o, Tissue-specific expression of βKlotho and fibroblast growth factor (FGF) receptor isoforms determines metabolic activity of FGF19 and FGF21. *J. Biol. Chem.* **282**, 26687–26695 (2007).
5. B. C. Lin, M. Wang, C. Blackmore, L. R. Desnoyers, Liver-specific activities of FGF19 require Klotho beta. *J. Biol. Chem.* **282**, 27277–27284 (2007).
6. D. Kimelman, M. Kirschner, Synergistic induction of mesoderm by FGF and TGF-β and the identification of an mRNA coding for FGF in the early Xenopus embryo. *Cell* **51**, 869–877 (1987).
7. R. Montesano, J. D. Vassalli, A. Baird, R. Guillemin, L. Orci, Basic fibroblast growth factor induces angiogenesis in vitro. *Proc. Natl. Acad. Sci. U.S.A.* **83**, 7297–7301 (1986).
8. S. Werner, H. Smola, X. Liao, M. T. Longaker, T. Krieg, P. H. Hofschneider, L. T. Williams, The function of KGF in morphogenesis of epithelium and reepithelialization of wounds. *Science* **266**, 819–822 (1994).
9. W. Risau, H. Sariola, H. G. Zerwes, J. Sasse, P. Ekblom, R. Kemler, T. Doetschman, Vasculogenesis and angiogenesis in embryonic-stem-cell-derived embryoid bodies. *Development* **102**, 471–478 (1988).
10. A. Beenken, M. Mohammadi, The FGF family: Biology, pathophysiology and therapy. *Nat. Rev. Drug Discov.* **8**, 235–253 (2009).
11. N. Turner, R. Grose, Fibroblast growth factor signalling: From development to cancer. *Nat. Rev. Cancer* **10**, 116–129 (2010).
12. A. J. Bass, H. Watanabe, C. H. Mermel, S. Yu, S. Perner, R. G. Verhaak, S. Y. Kim, L. Wardwell, P. Tamayo, I. Gat-Viks, A. H. Ramos, M. S. Woo, B. A. Weir, G. Getz, R. Beroukhim, M. O'Kelly, A. Dutt, O. Rozenblatt-Rosen, P. Dziunycz, J. Komisarof, L. R. Chirieac, C. J. Lafargue, V. Scheble, T. Wilbertz, C. Ma, S. Rao, H. Nakagawa, D. B. Stairs, L. Lin, T. J. Giordano, P. Wagner, J. D. Minna, A. F. Gazdar, C. Q. Zhu, M. S. Brose, I. Cecconello, U. Ribeiro Jr., S. K. Marie, O. Dahl, R. A. Shivdasani, M. S. Tsao, M. A. Rubin, K. K. Wong, A. Regev, W. C. Hahn, D. G. Beer, A. K. Rustgi, M. Meyerson, *SOX2* is an amplified lineage-survival oncogene in lung and esophageal squamous cell carcinomas. *Nat. Genet.* **41**, 1238–1242 (2009).
13. D. Cappellen, C. De Oliveira, D. Ricol, S. de Medina, J. Bourdin, X. Sastre-Garau, D. Chopin, J. P. Thiery, F. Radvanyi, Frequent activating mutations of FGFR3 in human bladder and cervix carcinomas. *Nat. Genet.* **23**, 18–20 (1999).
14. C. Greenman, P. Stephens, R. Smith, G. L. Dalgliesh, C. Hunter, G. Bignell, H. Davies, J. Teague, A. Butler, C. Stevens, S. Edkins, S. O'Meara, I. Vastrik, E. E. Schmidt, T. Avis, S. Barthorpe, G. Bhamra, G. Buck, B. Choudhury, J. Clements, J. Cole, E. Dicks, S. Forbes, K. Gray, K. Halliday, R. Harrison, K. Hills, J. Hinton, A. Jenkinson, D. Jones, A. Menzies, T. Mironenko, J. Perry, K. Raine, D. Richardson, R. Shepherd, A. Small, C. Tofts, J. Varian, T. Webb, S. West, S. Widaa, A. Yates, D. P. Cahill, D. N. Louis, P. Goldstraw, A. G. Nicholson, F. Brasseur, L. Looijenga, B. L. Weber, Y. E. Chiew, A. DeFazio, M. F. Greaves, A. R. Green, P. Campbell, E. Birney, D. F. Easton, G. Chenevix-Trench, M. H. Tan, S. K. Khoo, B. T. Teh, S. T. Yuen, S. Y. Leung, R. Wooster, P. A. Futreal, M. R. Stratton, Patterns of somatic mutation in human cancer genomes. *Nature* **446**, 153–158 (2007).
15. P. M. Pollock, M. G. Gartside, L. C. Dejeza, M. A. Powell, M. A. Mallon, H. Davies, M. Mohammadi, P. A. Futreal, M. R. Stratton, J. M. Trent, P. J. Goodfellow, Frequent activating FGFR2 mutations in endometrial carcinomas parallel germline mutations associated with craniosynostosis and skeletal dysplasia syndromes. *Oncogene* **26**, 7158–7162 (2007).
16. J. Weiss, M. L. Sos, D. Seidel, M. Peifer, T. Zander, J. M. Heuckmann, R. T. Ullrich, R. Menon, S. Maier, A. Soltermann, H. Moch, P. Wagener, F. Fischer, S. Heynck, M. Koker, J. Schöttle, F. Leenders, F. Gabler, I. Dabow, S. Querings, L. C. Heukamp, H. Balke-Want, S. Ansén, D. Rauh, I. Baessmann, J. Altmüller, Z. Wainer, M. Conron, G. Wright, P. Russell, B. Solomon, E. Brambilla, C. Brambilla, P. Lorimier, S. Sollberg, O. T. Brustugun, W. Engel-Riedel, C. Ludwig, I. Petersen, J. Sänger, J. Clement, H. Groen, W. Timens, H. Sietsma, E. Thunnissen, E. Smit, D. Heideman, F. Cappuzzo, C. Ligorio, S. Damiani, M. Hallek, R. Beroukhim, W. Pao, B. Klebl, M. Baumann, R. Buettner, K. Ernestus, E. Stoelben, J. Wolf, P. Nürnberg, S. Perner, R. K. Thomas, Frequent and focal *FGFR1* amplification associates with therapeutically tractable FGFR1 dependency in squamous cell lung cancer. *Sci. Transl. Med.* **2**, 62ra93 (2010).
17. H. Itoh, Y. Hattori, H. Sakamoto, H. Ishii, T. Kishi, H. Sasaki, T. Yoshida, M. Koono, T. Sugimura, M. Terada, Preferential alternative splicing in cancer generates a K-*sam* messenger RNA with higher transforming activity. *Cancer Res.* **54**, 3237–3241 (1994).
18. M. Chesi, E. Nardini, L. A. Brents, E. Schröck, T. Ried, W. M. Kuehl, P. L. Bergsagel, Frequent translocation t(4;14)(p16.3;q32.3) in multiple myeloma is associated with increased expression and activating mutations of fibroblast growth factor receptor 3. *Nat. Genet.* **16**, 260–264 (1997).
19. M. Peifer, L. Fernández-Cuesta, M. L. Sos, J. George, D. Seidel, L. H. Kasper, D. Plenker, F. Leenders, R. Sun, T. Zander, R. Menon, M. Koker, I. Dahmen, C. Müller, V. Di Cerbo, H. U. Schildhaus, J. Altmüller, I. Baessmann, C. Becker, B. de Wilde, J. Vandesompele, D. Böhm, S. Ansén, F. Gabler, I. Wilkening, S. Heynck, J. M. Heuckmann, X. Lu, S. L. Carter, K. Cibulskis, S. Banerji, G. Getz, K. S. Park, D. Rauh, C. Grütter, M. Fischer, L. Pasqualucci, G. Wright, Z. Wainer, P. Russell, I. Petersen, Y. Chen, E. Stoelben, C. Ludwig, P. Schnabel, H. Hoffmann, T. Muley, M. Brockmann, W. Engel-Riedel, L. A. Muscarella, V. M. Fazio, H. Groen, W. Timens, H. Sietsma, E. Thunnissen, E. Smit, D. A. Heideman, P. J. Snijders, F. Cappuzzo, C. Ligorio, S. Damiani, J. Field, S. Solberg, O. T. Brustugun, M. Lund-Iversen, J. Sänger, J. H. Clement, A. Soltermann, H. Moch, W. Weder, B. Solomon, J. C. Soria, P. Validire, B. Besse, E. Brambilla, C. Brambilla, S. Lantuejoul, P. Lorimier, P. M. Schneider, M. Hallek, W. Pao, M. Meyerson, J. Sage, J. Shendure, R. Schneider, R. Büttner, J. Wolf, P. Nürnberg, S. Perner, L. C. Heukamp, P. K. Brindle, S. Haas, R. K. Thomas, Integrative genome analyses identify key somatic driver mutations of small-cell lung cancer. *Nat. Genet.* **44**, 1104–1110 (2012).
20. A. Dutt, A. H. Ramos, P. S. Hammerman, C. Mermel, J. Cho, T. Sharifnia, A. Chande, K. E. Tanaka, N. Stransky, H. Greulich, N. S. Gray, M. Meyerson, Inhibitor-sensitive *FGFR1* amplification in human non-small cell lung cancer. *PLoS One* **6**, e20351 (2011).
21. A. Dutt, H. B. Salvesen, T. H. Chen, A. H. Ramos, R. C. Onofrio, C. Hatton, R. Nicoletti, W. Winckler, R. Grewal, M. Hanna, N. Wyhs, L. Ziaugra, D. J. Richter, J. Trovik, I. B. Engelsen, I. M. Stefansson, T. Fennell, K. Cibulskis, M. C. Zody, L. A. Akslen, S. Gabriel, K. K. Wong, W. R. Sellers, M. Meyerson, H. Greulich, Drug-sensitive *FGFR2* mutations in endometrial carcinoma. *Proc. Natl. Acad. Sci. U.S.A.* **105**, 8713–8717 (2008).
22. A. O. Wilkie, S. J. Patey, S. H. Kan, A. M. van den Ouweland, B. C. Hamel, FGFs, their receptors, and human limb malformations: Clinical and molecular correlations. *Am. J. Med. Genet.* **112**, 266–278 (2002).
23. O. A. Ibrahimi, A. V. Eliseenkova, A. N. Plotnikov, K. Yu, D. M. Ornitz, M. Mohammadi, Structural basis for fibroblast growth factor receptor 2 activation in Apert syndrome. *Proc. Natl. Acad. Sci. U.S.A.* **98**, 7182–7187 (2001).
24. H. D. Sun, M. Malabunga, J. R. Tonra, R. DiRenzo, F. E. Carrick, H. Zheng, H. R. Berthoud, O. P. McGuinness, J. Shen, P. Bohlen, R. L. Leibel, P. Kussie, Monoclonal antibody antagonists of hypothalamic FGFR1 cause potent but reversible hypophagia and weight loss in rodents and monkeys. *Am. J. Physiol. Endocrinol. Metab.* **292**, E964–E976 (2007).
25. A. P. Brown, C. L. Courtney, L. M. King, S. C. Groom, M. J. Graziano, Cartilage dysplasia and tissue mineralization in the rat following administration of a FGF receptor tyrosine kinase inhibitor. *Toxicol. Pathol.* **33**, 449–455 (2005).
26. V. Guagnano, P. Furet, C. Spanka, V. Bordas, M. Le Douget, C. Stamm, J. Brueggen, M. R. Jensen, C. Schnell, H. Schmid, M. Wartmann, J. Berghausen, P. Drueckes, A. Zimmerlin, D. Bussiere, J. Murray, D. Graus Porta, Discovery of 3-(2,6-dichloro-3,5-dimethoxy-phenyl)-1-{6-[4-(4-ethyl-piperazin-1-yl)-phenylamino]-pyrimidin-4-yl}-1-methyl-urea (NVP-BGJ398), a potent and selective inhibitor of the fibroblast growth factor receptor family of receptor tyrosine kinase. *J. Med. Chem.* **54**, 7066–7083 (2011).
27. P. R. Gavine, L. Mooney, E. Kilgour, A. P. Thomas, K. Al-Kadhimi, S. Beck, C. Rooney, T. Coleman, D. Baker, M. J. Mellor, A. N. Brooks, T. Klinowska, AZD4547: An orally bioavailable, potent, and selective inhibitor of the fibroblast growth factor receptor tyrosine kinase family. *Cancer Res.* **72**, 2045–2056 (2012).
28. The ADHR Consortium, Autosomal dominant hypophosphataemic rickets is associated with mutations in FGF23. *Nat. Genet.* **26**, 345–348 (2000).
29. T. Shimada, M. Kakitani, Y. Yamazaki, H. Hasegawa, Y. Takeuchi, T. Fujita, S. Fukumoto, K. Tomizuka, T. Yamashita, Targeted ablation of *Fgf23* demonstrates an essential physiological role of FGF23 in phosphate and vitamin D metabolism. *J. Clin. Invest.* **113**, 561–568 (2004).
30. D. E. Johnson, L. T. Williams, Structural and functional diversity in the FGF receptor multigene family. *Adv. Cancer Res.* **60**, 1–41 (1993).
31. X. Zhang, O. A. Ibrahimi, S. K. Olsen, H. Umemori, M. Mohammadi, D. M. Ornitz, Receptor specificity of the fibroblast growth factor family. The complete mammalian FGF family. *J. Biol. Chem.* **281**, 15694–15700 (2006).
32. N. Itoh, Hormone-like (endocrine) Fgfs: Their evolutionary history and roles in development, metabolism, and disease. *Cell Tissue Res.* **342**, 1–11 (2010).

33. H. H. Fiebig, A. M. Burger, *Relevance of Tumor Models for Anticancer Drug Development* (Karger AG, Basel, 1999).
34. U. McDermott, R. Y. Ames, A. J. Iafrate, S. Maheswaran, H. Stubbs, P. Greninger, K. McCutcheon, R. Milano, A. Tam, D. Y. Lee, L. Lucien, B. W. Brannigan, L. E. Ulkus, X. J. Ma, M. G. Erlander, D. A. Haber, S. V. Sharma, J. Settleman, Ligand-dependent platelet-derived growth factor receptor (PDGFR)-α activation sensitizes rare lung cancer and sarcoma cells to PDGFR kinase inhibitors. *Cancer Res.* **69**, 3937–3946 (2009).
35. A. H. Ramos, A. Dutt, C. Mermel, S. Perner, J. Cho, C. J. Lafargue, L. A. Johnson, A. C. Stiedl, K. E. Tanaka, A. J. Bass, J. Barretina, B. A. Weir, R. Beroukhim, R. K. Thomas, J. D. Minna, L. R. Chirieac, N. I. Lindeman, T. Giordano, D. G. Beer, P. Wagner, I. I. Wistuba, M. A. Rubin, M. Meyerson, Amplification of chromosomal segment 4q12 in non-small cell lung cancer. *Cancer Biol. Ther.* **8**, 2042–2050 (2009).
36. D. M. Ornitz, J. Xu, J. S. Colvin, D. G. McEwen, C. A. MacArthur, F. Coulier, G. Gao, M. Goldfarb, Receptor specificity of the fibroblast growth factor family. *J. Biol. Chem.* **271**, 15292–15297 (1996).
37. A. Tolcher, K. Papadopolous, A. Patniak, E. Heath, A. Weise, T. Prokop, S. Morrone, J. Zanghi, H. N. Keer, P. LoRusso, Preliminary results of a dose escalation study of the fibroblast growth factor (FGF) "trap" FP-1039 (FGFR1:Fc) in patients with advanced malignancies, *Proceedings of the 22nd EORTC-NCI-AACR Symposium on Molecular Targets and Cancer Therapeutics*, 2010.
38. M. S. Pepper, N. Ferrara, L. Orci, R. Montesano, Potent synergism between vascular endothelial growth factor and basic fibroblast growth factor in the induction of angiogenesis in vitro. *Biochem. Biophys. Res. Commun.* **189**, 824–831 (1992).
39. A. Compagni, P. Wilgenbus, M. A. Impagnatiello, M. Cotten, G. Christofori, Fibroblast growth factors are required for efficient tumor angiogenesis. *Cancer Res.* **60**, 7163–7169 (2000).
40. M. E. Marshall, T. K. Hinz, S. A. Kono, K. R. Singleton, B. Bichon, K. E. Ware, L. Marek, B. A. Frederick, D. Raben, L. E. Heasley, Fibroblast growth factor receptors are components of autocrine signaling networks in head and neck squamous cell carcinoma cells. *Clin. Cancer Res.* **17**, 5016–5025 (2011).
41. S. Lee, Y. Kim, J. M. Sun, Y. L. Choi, J. G. Kim, Y. M. Shim, Y. H. Park, J. S. Ahn, K. Park, J. H. Han, M. J. Ahn, Molecular profiles of EGFR, K-ras, c-met, and FGFR in pulmonary pleomorphic carcinoma, a rare lung malignancy. *J. Cancer Res. Clin. Oncol.* **137**, 1203–1211 (2011).
42. N. C. Turner, M. J. Seckl, A therapeutic target for smoking-associated lung cancer. *Sci. Transl. Med.* **2**, 62ps56 (2010).
43. J. Running Deer, D. S. Allison, High-level expression of proteins in mammalian cells using transcription regulatory sequences from the Chinese hamster EF-1α gene. *Biotechnol. Prog.* **20**, 880–889 (2004).

Acknowledgments: We acknowledge the excellent technical assistance of S. Giese, D. Chau, T. Bray, A. K. Hsu, J. Powers, H. Kaur, E. Bosch, R. Cheung, and M. Aguirre (Five Prime Therapeutics Inc.). **Author contributions:** T.C.H., A.S., and A.L. performed in vitro experiments and qRT-PCR analysis. L.L., H.Z., and S.P. performed xenograft tumor analysis and FGFR signaling analysis. K.H. ran all bioinformatic and statistical analysis. J.Z. and N.P. performed bioanalytical analysis. A.W.H. and R.H. performed all SPR analysis. S.A.M., D.C., and M.Q. designed and produced FP-1039 protein. T.B., S.K.D., D.H., W.M.K., L.T.W., and K.P.B. supervised and directed the research. T.C.H., L.T.W., and K.P.B. wrote and edited the manuscript. **Competing interests:** All authors are current or former employees of Five Prime Therapeutics Inc., a privately held biotechnology company, and have received monetary compensation and stock options as a result of employment by the company. D.H., M.Q., and A.S. have been granted U.S. Patent 7,678,890 entitled "Compositions and methods of treating disease with FGFR fusion proteins" that encompasses research outlined in this paper.

Submitted 28 November 2012
Accepted 29 January 2013
Published 27 March 2013
10.1126/scitranslmed.3005414

Citation: T. C. Harding, L. Long, S. Palencia, H. Zhang, A. Sadra, K. Hestir, N. Patil, A. Levin, A. W. Hsu, D. Charych, T. Brennan, J. Zanghi, R. Halenbeck, S. A. Marshall, M. Qin, S. K. Doberstein, D. Hollenbaugh, W. M. Kavanaugh, L. T. Williams, K. P. Baker, Blockade of nonhormonal fibroblast growth factors by FP-1039 inhibits growth of multiple types of cancer. *Sci. Transl. Med.* **5**, 178ra39 (2013).